Open-Boundary Molecular Dynamics of a DNA Molecule in a Hybrid Explicit/Implicit Salt Solution

Julija Zavadlav,[1] Jurij Sablić,[2] Rudolf Podgornik,[3,4] and Matej Praprotnik[2,4,*]

[1]Computational Science & Engineering Laboratory, ETH Zurich, Zurich, Switzerland; [2]Laboratory for Molecular Modeling, National Institute of Chemistry, Ljubljana, Slovenia; [3]Theoretical Physics Department, J. Stefan Institute, Ljubljana, Slovenia; and [4]Department of Physics, Faculty of Mathematics and Physics, University of Ljubljana, Ljubljana, Slovenia

ABSTRACT The composition and electrolyte concentration of the aqueous bathing environment have important consequences for many biological processes and can profoundly affect the behavior of biomolecules. Nevertheless, because of computational limitations, many molecular simulations of biophysical systems can be performed only at specific ionic conditions: either at nominally zero salt concentration, i.e., including only counterions enforcing the system's electroneutrality, or at excessive salt concentrations. Here, we introduce an efficient molecular dynamics simulation approach for an atomistic DNA molecule at realistic physiological ionic conditions. The simulations are performed by employing the open-boundary molecular dynamics method that allows for simulation of open systems that can exchange mass and linear momentum with the environment. In our open-boundary molecular dynamics approach, the computational burden is drastically alleviated by embedding the DNA molecule in a mixed explicit/implicit salt-bathing solution. In the explicit domain, the water molecules and ions are both overtly present in the system, whereas in the implicit water domain, only the ions are explicitly present and the water is described as a continuous dielectric medium. Water molecules are inserted and deleted into/from the system in the intermediate buffer domain that acts as a water reservoir to the explicit domain, with both water molecules and ions free to enter or leave the explicit domain. Our approach is general and allows for efficient molecular simulations of biomolecules solvated in bathing salt solutions at any ionic strength condition.

INTRODUCTION

The structure, stability, dynamics, and function of biological macromolecules are, apart from their specific chemical composition, profoundly affected by their bathing environment, i.e., the aqueous electrolyte solution. This electrolyte environment is especially important in biological systems (1) involving strong negatively charged biomolecules such as nucleic acids (2) or zwitterionic macromolecules such as proteins (3). Indeed, there are many different manifestations of the role of the bathing solution, including molecular recognition, DNA packing in viral and cellular compartments, RNA and viral capsid protein coassembly, RNA and protein folding, and DNA condensation driven by the counterintuitive like-charge attraction (4–7). Biomolecules in their turn strongly influence the surrounding aqueous solvent that exhibits local structure and dynamics that differ significantly from bulk-like behavior (8–11), some-

times creating an indistinguishable macromolecule-solvent conglomerate (12).

These examples all specifically underline the importance of careful modeling of the aqueous solution in molecular dynamics (MD) simulations of biological systems, which need to take into account the details of the hydration layer at the atomistic resolution as well as physiologically relevant solution ionic strength. Nevertheless, for practical and computational reasons, many simulations of, e.g., DNA, still only explicitly include the neutralizing counterions, skirting altogether the effect of the salt at physiological conditions (13). In particular, for statistical reasons, the latter case stipulates a sufficiently large number of salt ions such that the bulk-like behavior of ions emerges in the distal ionic solution, far away from the DNA. Thus, the challenge of small, physiologically relevant ionic concentrations (approximately 0.15 M) resides in rather huge simulation systems that cannot be dealt with without resorting to substantial super-computer power; thus, they remain often beyond reach for all-atom simulations.

These limitations can be circumvented with multiscale methods (14) such as Adaptive Resolution Scheme

(AdResS) [15–19] or its extensions, e.g., the grand-canonical-like version [20–23] and the Hamiltonian version [24–28]. There, the all-atom resolution is preserved only in the physically relevant part of the system, whereas the remainder is modeled with a simplified coarse-grained (CG) representation, in which certain degrees of freedom that are deemed irrelevant are integrated out [29–33]. Thus far, AdResS has been applied to many biophysical systems, ranging from pure solvents [24,34–37] and ionic liquids [38,39] to systems containing fullerene [40], protein [41–44], single DNA [8,45], and many DNA arrays [46]. The computational efficiency is gained on account of the CG region and thus depends on the size of the CG region, the level of CG, and the employed force field [47]. The most extreme case, therefore, corresponds to the CG model with no intermolecular interactions, i.e., an ideal gas [48] or an implicit salt solution [49–52]. Because the particles in AdResS can freely diffuse across the resolution domains, the CG region can be seen as a particle reservoir. It is important to note that in these systems the overall simulation is still performed in the canonical ensemble (the number of particles is fixed), and therefore, the system as a whole does not exchange matter with an external environment. Molecular simulations of small open-boundary systems [18,53], which can exchange mass, energy, and momentum with their surroundings, are closely related to the emerging area of stochastic thermodynamics. The latter extends the traditional laws of thermodynamics to microscopic systems in which thermal and quantum fluctuations cannot be ignored [54–57].

To perform truly open molecular simulations, one can employ open-boundary molecular dynamics (OBMD) [58–61], which permits simulations in the grand canonical ensemble. The OBMD method combines features of AdResS and open MD [62,63], which enables the exchange of energy, momentum, and matter with the external environment through the imposed arbitrary time-dependent external pressure tensor. To this end, a buffer domain is introduced, which acts as a mass and momentum reservoir for the explicit domain, located in the region where the behavior of molecules is bulk-like. In molecular simulations of a DNA molecule in salt solution, water can be considered as a dielectric continuum from the second DNA coordination shell onward, whereas the fluctuating cloud of ions surrounding the DNA, the so-called ionic atmosphere [4,64–67], extends to a wider region. Therefore, to perform OBMD simulations that include also the ions, one needs to consider larger all-atom regions that would eventually undermine the original idea of an efficient simulation.

To preserve the efficiency of the simulations, we perform MD of a single DNA molecule solvated in a bathing salt solution by using OBMD for the water molecules and the AdResS method for the ions (see Fig. 1). The domain containing explicit molecules (DNA + water + ions) is open, i.e., not periodic, and the water molecules are deleted and inserted at the boundary buffer domain. The implicit water domain still contains explicit ions with screened electrostatics. The interaction coupling for ions is carried out by AdResS and in contradistinction to water molecules, the total number of ions in the whole simulation box remains constant [34]. Our method thus couples the explicit all-atom salt solution used in the cylindrical layer surrounding the DNA and the implicit water with explicit ions used in the outer part of the simulation box, which can be vastly increased with miniature computational overhead. In this work, the DNA molecule is immersed in a monovalent salt solution. However, using the same methodology, other solution environments can also be envisioned to study other biologically relevant processes, e.g., phase transition between the hexagonal and the orthorhombic phases of dense DNA arrays with either monovalent or multivalent (spermidine) counterions [46,68]. There, a more elaborated comparison with the experimental data is described, and the experimental osmotic pressure (equation of state) is specifically compared with the calculated one. In simulations, the osmotic pressure test is typically much more stringent than any other comparison. The biophysical importance of the equation of the state of DNA has been described at length in, e.g., [69]. Contrary to the mentioned works, our current work is dedicated specifically to advances in the simulation methodology.

METHODS

The simulated system of a DNA molecule embedded in the coupled explicit/implicit salt solution is schematically depicted in Figs. 1 and 2. The DNA molecule is always modeled at the full atomistic resolution using the Assisted Model Building with Energy Refinement (AMBER) force field [70], with the center of the explicit region coinciding with the DNA's center of mass (CoM). The solvent's level of representation depends on the distance from the DNA. At short distances, water is modeled with an atomistic transferable intermolecular potential with three points (TIP3P) [71] water model, whereas the AMBER force field parameters are used for the ions. Distal water is considered implicitly as a dielectric continuum (the implicit water region). There, the ions have the same Lennard-Jones interaction parameters and the same charges as in the explicit region. Thus, the ion-ion interactions are equal in both regions, except for the additional dielectric screening of the electrostatic interactions in the implicit region [8,34]. In between the explicit and implicit water domains, there is a buffer region that acts as a reservoir where new water molecules are inserted, allowing the explicit domain to exchange mass, momentum, and energy through its boundary with the buffer. Water molecules that exit the buffer region into the implicit water domain are deleted. The geometrical boundaries between all regions are cylinders, as this shape adequately reflects the local structure of the DNA molecule. Obviously, by construction, this model cannot deal with mesoscale conformational fluctuations of the DNA chain in the bathing solution but can certainly adequately represent microscopic fluctuations of the DNA heavy atoms with respect to a reference structure.

The total force acting on a molecule α is [58]

$$\mathbf{F}_{\alpha} = \mathbf{F}_{\alpha}^{AdResS} + \mathbf{F}_{\alpha}^{ext} + \mathbf{F}_{\alpha}^{thermo}. \tag{1}$$

The adaptive resolution force $\mathbf{F}^{AdResS}$ accounts for the implicit/explicit resolution change, the external force $\mathbf{F}^{ext}$ imposes the desired external pressure
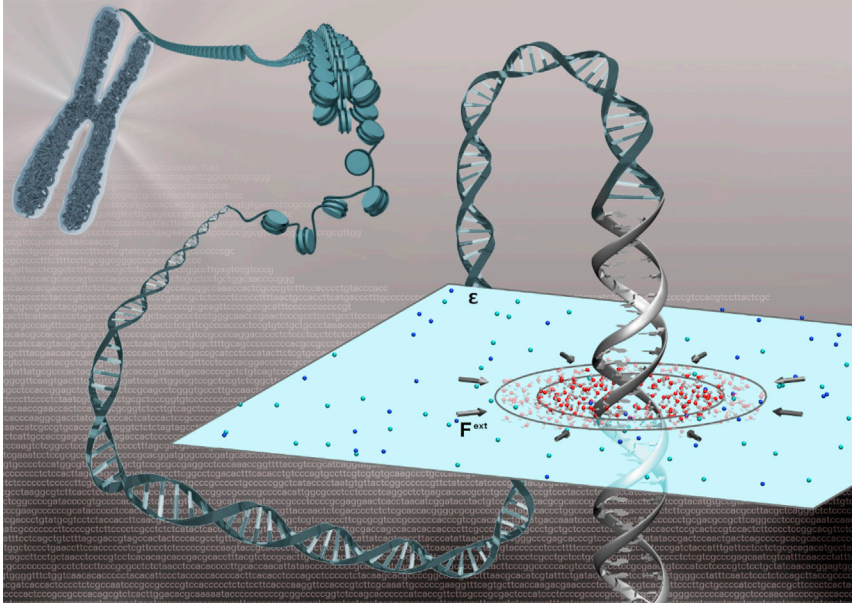
FIGURE 1 Schematic representation of the atomistic DNA molecule embedded in the coupled explicit/implicit salt solution using the open-boundary adaptive resolution simulation scheme. To see this figure in color, go online.

tensor, and $\mathbf{F}^{thermo}$ is the thermostat contribution (see below). The AdResS contribution on a molecule α is given by

$$
\begin{aligned}
\mathbf{F}_{\alpha}^{AdResS} &= \sum_{\beta \neq \alpha} w(|\mathbf{R}_{\alpha} - \mathbf{R}|)w(|\mathbf{R}_{\beta} - \mathbf{R}|)\mathbf{F}_{\alpha\beta}^{ex} + \\
&\quad \sum_{\beta \neq \alpha}[1 - w(|\mathbf{R}_{\alpha} - \mathbf{R}|)w(|\mathbf{R}_{\beta} - \mathbf{R}|)]\mathbf{F}_{\alpha\beta}^{im} \quad (2) \\
&\quad - \mathbf{F}_{\alpha}^{TD}(|\mathbf{R}_{\alpha} - \mathbf{R}|),
\end{aligned}
$$

where $\mathbf{F}_{\alpha\beta}^{ex}$ and $\mathbf{F}_{\alpha\beta}^{im}$ are the forces between molecules α and β, obtained from the explicit all-atom and implicit potentials, respectively. $\mathbf{F}_{\alpha\beta}^{ex} = \sum_{i \in \alpha, j \in \beta} \mathbf{F}_{i\alpha j\beta}^{ex} = -\nabla_{\mathbf{r}_{ij}} U^{ex}(\mathbf{r}_{ij})$, where the sum runs over all pair interactions between atom i of the molecule α and atom j of the molecule β. Note that $\mathbf{F}_{\alpha\beta}^{im} \neq 0$ only for the ion-ion interactions. The sigmoidal function w is used to smoothly couple the implicit/explicit regimes. It is equal to 1 and 0 in the explicit and implicit water domains, respectively. In the hybrid region, $w \in [0,1]$, as depicted in Fig. 2. There, the resolution is gradually switched from the explicit to the implicit, whereas the molecules freely move between different domains. Note that the hybrid domain overlaps with the buffer domain. $\mathbf{R}_{\alpha}$, $\mathbf{R}_{\beta}$, and $\mathbf{R}$ are two-dimensional (x,y) vectors of the CoMs of molecules α and β and the DNA (center of the simulation box in the case of the salt solution), respectively. The thermodynamic (TD) force $\mathbf{F}_{\alpha}^{TD}$ acts on the CoMs of the molecules in the hybrid region and enforces a uniform density profile by compensating the chemical potential differences between the implicit and explicit resolution molecular models (17,72,73). It is defined as a negative gradient of the effective excess chemical potential. Numerically, this translates into an iterative formula (17,73) $\mathbf{F}_{\alpha}^{TD^{i+1}} = \mathbf{F}_{\alpha}^{TD^{i}} - C\nabla\rho^{i}$, where C is an appropriately chosen numerical prefactor. The TD force depends on the molecule type, i.e., we use two different ones that correspond to sodium and chloride ions (8,34,74). For water, we set $\mathbf{F}_{water}^{TD} = 0$.

Water molecules are deleted once they leave the outer boundary of a buffer B and new water molecules are inserted according to the desired average density in the buffer. The mass balance is controlled by a feedback algorithm, $\Delta N_{B} = (\Delta t / \tau_{r})(\alpha\langle N_{B}\rangle - N_{B})$, where $\langle N_{B}\rangle$ and N_{B} are the average and the current number of molecules in the buffer, α is the user-defined parameter, whereas τ_{r} is the characteristic relaxation time of the buffer. New molecules are inserted if $\Delta N_{B} > 0$. We insert atomistically resolved water molecules. Thus, the insertion is carried out by the rotational

variant of the USHER iterative algorithm (75), which is a Newton-Raphson-like search method on the potential energy surface of the translational and rotational molecular degrees of freedom. However, we insert them in the buffer domain, which, as mentioned, overlaps with the hybrid domain, and there the forces are, according to AdResS, interpolated between the explicit all-atom and the implicit forces (for water, $\mathbf{F}_{\alpha\beta}^{im} = 0$; therefore, $\mathbf{F}_{\alpha}^{AdResS} = \sum_{\beta \neq \alpha} w(|\mathbf{R}_{\alpha} - \mathbf{R}|)w(|\mathbf{R}_{\beta} - \mathbf{R}|)\mathbf{F}_{\alpha\beta}^{ex}$). Hence, the interactions of inserted water molecules with surrounding molecules are softer than in the explicit region.

The external boundary conditions are imposed on water molecules via $\mathbf{F}^{ext}$, computed from the momentum flux balance as follows:

$$
\mathbf{F}^{ext} = \mathbf{J} \cdot \mathbf{n}_{B}A + \frac{\mathbf{P}_{out} - \mathbf{P}_{in}}{\Delta t} + \sum_{\alpha} \mathbf{F}_{\alpha}^{TD}, \quad (3)
$$

where $\mathbf{P}_{out}$ and $\mathbf{P}_{in}$ represent the total linear momenta of the water molecules that were removed and inserted into the simulation in the last time step of integration Δt. $\mathbf{J}$ is the momentum flux tensor that one would like to impose across the boundary of surface area A, and $\mathbf{n}_{B}$ is the unit vector normal to the buffer interface (see Fig. 2). The last term is the total cumulative TD force applied to the system. The external force defined in this manner (Eq. 3) ensures that the total linear momentum and energy are conserved (see Conservation of Linear Momentum). The total external force is distributed among the water molecules in the buffer $\mathbf{F}^{ext} = \sum_{\alpha \in B} \mathbf{F}_{\alpha}^{ext}$ with $\mathbf{F}_{\alpha}^{ext} = (m_{\alpha}/\sum_{\alpha \in B} m_{\alpha})\mathbf{F}^{ext}$ (58), where index α runs over all water molecules in the buffer region and $\mathbf{F}_{ions}^{ext} = 0$.

We use the dissipative particle dynamics (DPD) thermostat given by

$$
\mathbf{F}_{\alpha}^{thermo} = \sum_{i \in \alpha, j \in \beta, \beta \neq \alpha} \sigma\omega^{R}(r_{ij})\zeta_{ij}\widehat{\mathbf{r}}_{ij} - \gamma\omega^{D}(r_{ij})(\widehat{\mathbf{r}}_{ij} \cdot \mathbf{v}_{ij})\widehat{\mathbf{r}}_{ij},
$$

$$(4)$$

where the sum runs over all pair interactions between atom i of the molecule α and atom j of the molecule β, ζ_{ij} is a random variable with a Gaussian distribution, and unit variance and distance-dependent weight functions ω^{R} and ω^{D} are related via the fluctuation-dissipation theorem as $\omega^{D}(r_{ij}) = [\omega^{R}(r_{ij})]^{2} = (1 - r_{ij}/r_{c})$ for $r_{ij} < r_{c}$ and $\sigma^{2} = 2k_{B}T\gamma$.

Our OBMD for water is distinctive from the AdResS approach for coupling an all-atom force field to an ideal gas (48) because the water
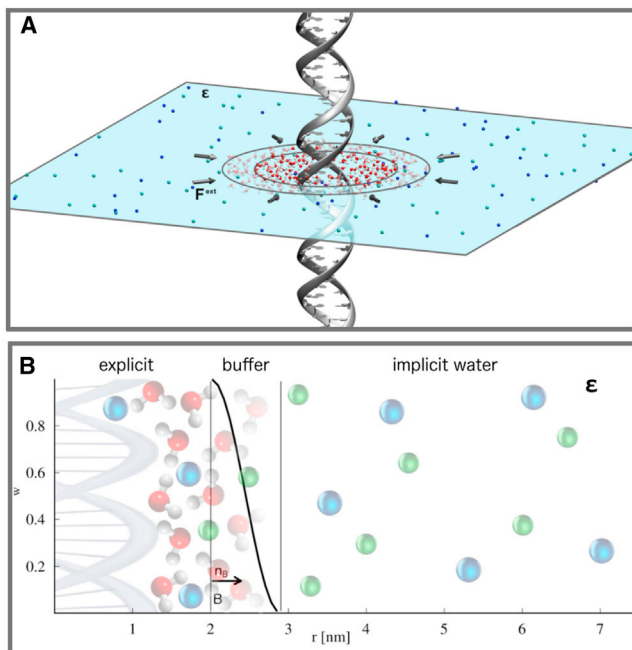
FIGURE 2 (A) A depiction of the simulation box with cylindrical resolution regions. The DNA, modeled at all times at the atomistic resolution, is surrounded by a cylindrical layer of explicit all-atom salt solution (the explicit domain). Distal water in the implicit water domain is modeled as a continuous dielectric medium, whereas the ions are still explicit. The water molecules are deleted if they enter the implicit water region and are inserted in the buffer region. To assist the insertion of water molecules and to provide a continuous transition from the explicit to implicit water domain of the ions, the explicit/implicit forces are interpolated in the buffer region according to the AdResS scheme. (B) A cross-section of the half of the simulation box that shows the boundaries between the resolution domains is displayed. To see this figure in color, go online.

molecules are deleted and inserted from/into the system. Furthermore, we do not employ a TD force on the water molecules, but we employ a linear-momentum-preserving external force. Our approach is also distinctive from the open MD (62,63) because the water molecules are not inserted directly into the explicit all-atom domain. Instead, they are inserted in the intermediate hybrid region, where the interactions are determined by the AdResS coupling scheme, i.e., they are softer, which accommodates for an easier insertion.

All MD simulations are performed using the ESPResSo++ software package (76). For the integration, we use a standard velocity Verlet integrator with a time step of 1 fs. We use an orthorhombic simulation box with periodic boundary conditions and minimal image convention. The simulation box size is $15 \times 15 \times 3.4$ nm^3. Thus, in the z direction, this corresponds to exactly one DNA pitch. The temperature is maintained at 300 K with the value of the friction constant at $\gamma = 0.2$ a.u./ps. The hydrogen atoms of the DNA molecule are constrained with the RATTLE (77) algorithm, whereas the geometry of water molecules is constrained with SETTLE (78). The nonbonded interactions are calculated with the Lennard-Jones and Coulomb interactions within a cutoff distance of 0.9 nm. The generalized reaction field method (79) is used for the electrostatic interaction beyond the cutoff, with a dielectric permittivity of outer region equal to 80 and the inverse Debye screening length $\kappa = 1.0$ and 3.25/nm corresponding to a 0.15 and 1.0 M salt solution, respectively. The dielectric permittivities of the inner region—that is, within cutoff distance—are equal to 1 and 80 for the explicit and implicit water regions, respectively. The size of the explicit cylinder radius is set to 2.0 nm, whereas the width of the buffer region is 0.9 nm. For the pure water and

salt solution systems, the production runs are 15 ns long after a 1-ns-long equilibration. For the DNA simulations, we first run a 100-ps-long simulation with constrained DNA atoms and ions to obtain the equilibrium water density profile and then a 100 ps simulation with constrained DNA atoms, followed by a 1 ns equilibration without constraints. The first two equilibrations are performed with the Langevin instead of the DPD thermostat to damp any preexisting sound waves in the system (58). The production runs are 20 ns. The DNA simulations are compared with the reference full-blown atomistic simulation at 1 M NaCl salt solution reported in (8).

RESULTS AND DISCUSSION

Open-boundary multiscale solvation

As shown in several previous publications (18,58–61), the OBMD equilibrium simulation samples the grand canonical ensemble even if the total number of ions in the whole simulation box remains constant. The explicit region thus acts as an open system that exchanges mass with its surroundings. In the TD limit, the mass variance σ_M is related to the isothermal sound velocity c_T through $\sigma_M^2/V = \rho k_B T/c_T^2$, where V is the volume of the considered system. The c_T can be evaluated using the pressure equation of state or isothermal compressibility β_T, i.e., $c_T^2 = (\partial p/\partial \rho)_T = (\beta_T \rho)^{-1}$. In Table 1, we report the calculated water mass variance inside the explicit domain for the pure water system and for the two salt solutions. Taking $\beta_T = 57.4 \times 10^{-6}$ /bar and $\rho = 1.017$ g/cm^3 for the TIP3P water reported in (80), the grand canonical prediction is $\sigma_M^2/V = 886$ a.u. (2) nm^{-3}. For all systems, the obtained values for water are in quite good agreement with the prediction. Thus, the subsystem of water is behaving grand canonically. The ions are technically simulated in the canonical ensemble. However, it was shown that the explicit region within the AdResS simulation approaches the grand-canonical-like behavior provided that the surrounding regions, e.g., buffer and implicit/CG domains, are sufficiently large (20,21). Furthermore, even if the OBMD setup were used for the ions, one could not expect to obtain the TD limit of grand canonical ensemble, largely because of their small number.

Next, we compute in Fig. 3 the water normalized density profile (NDP) in the radial direction in which the system is open. The profiles are normalized with the desired density ρ_w of the TIP3P water model. Within the explicit region, NDPs are flat for all three considered solvations, actually decreasing with molarity as the average density of water

TABLE 1 Water Mass Variance for the Explicit Domain for the Pure Water System and NaCl Salt Solution at 0.15 and 1.0 M Molarities

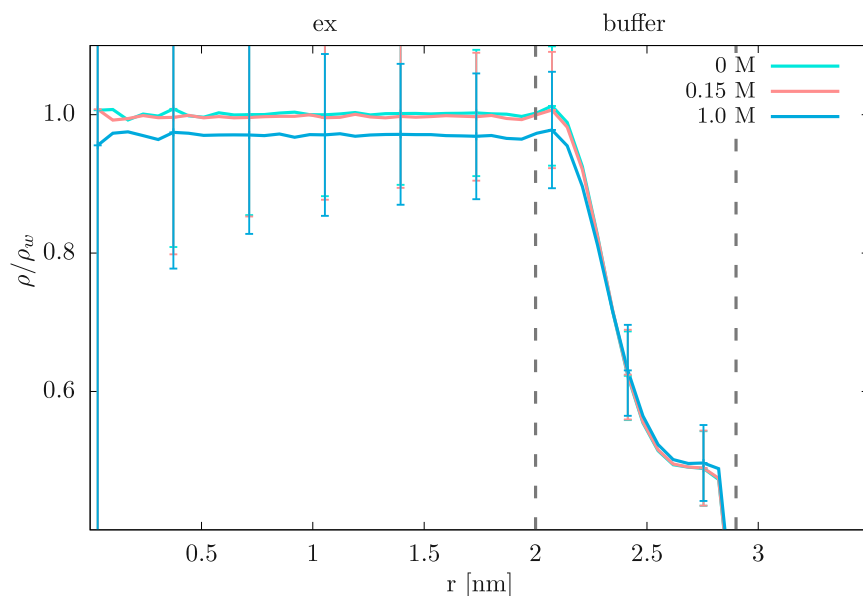| NaCl Salt Molarity	σ_M^2/V (ex) [a.u.^{2}nm^{-3}]
0.00	814
0.15	861
1.00	995

Error bars are ∼5%.

FIGURE 3 Normalized density profiles for water. The results are shown for the pure water system (0 M) and NaCl salt solution at concentrations 0.15 and 1.0 M. The error bars and vertical gray lines denote the SD and resolution region boundaries, respectively. To see this figure in color, go online.

is decreased because of the presence of ions. Within the buffer domain between the explicit and implicit regions, the density gradually decreases for larger radii depending on the details of the user-selected parameters of the insertion algorithm, such as α (we use $\alpha = 0.7$) and the imposed external pressure (1 bar). The NDPs (normalized with the salt density ρ_s given by a molar concentration) for sodium and chloride ions for both considered molar concentrations are shown in Fig. 4. In AdResS simulations, the molecules typically drift toward the region with lower chemical poten-

tial. To effectively correct the unwanted density undulations, the TD force is applied (17,35,73). For ions, these effects are drastically more pronounced than for water (8,74). To demonstrate this point, we plot in Fig. 4 additional NDPs for ions where the TD force has been omitted. The use of the TD force thus cannot be avoided for ions. However, for the water, which comprises a majority of the system, the TD force is not required. The TD forces are obtained with an iterative procedure described in detail in (17,35,73) and act on ions in the buffer domain. With the
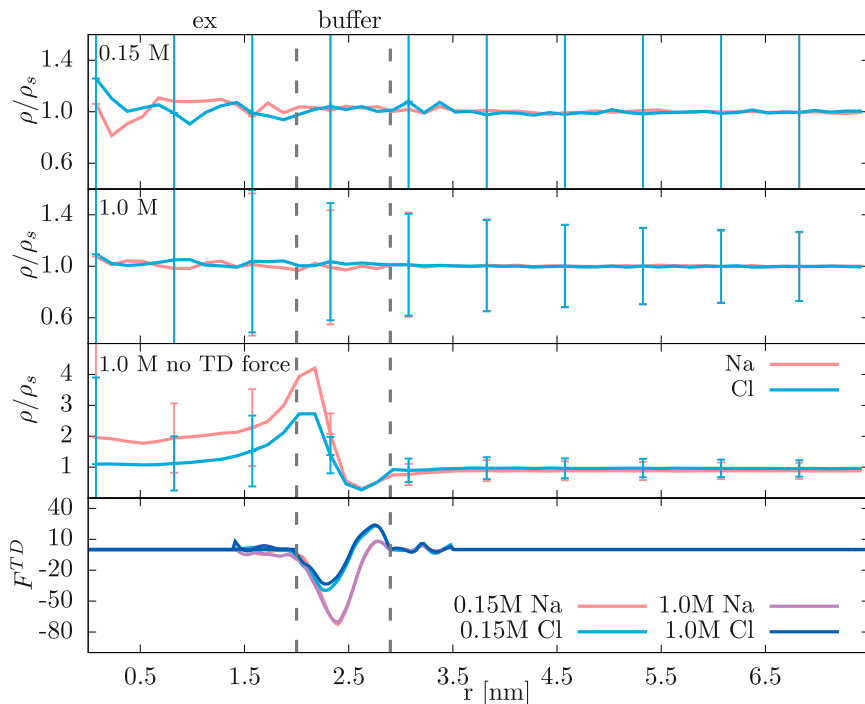

FIGURE 4 Top: normalized density profiles for sodium (Na) and chloride (Cl) ions for 0.15 and 1.0 M with and without the TD forces. Bottom: TD forces (in units of kJ mol^{-1}nm^{-1}) are shown for both ion types that act mainly in the buffer region. Vertical gray lines mark the resolution region boundaries. To see this figure in color, go online.

TD force employed, the obtained NDPs for the ions are also flat. Due to statistics, larger variations are observed for the 0.15 M salt solution.

The positional water-water and water-ion correlations are characterized by the corresponding radial distribution functions (RDFs), which are shown in Fig. 5. For the oxygen-oxygen RDFs, we observe the known effect of adding salt, i.e., the water structure is similarly modified as under increased pressure. In particular, the first peak weakens, whereas the second peak moves inwards (34,81).

Conservation of linear momentum

As already mentioned above, the OBMD simulation technique conserves the linear momentum. The DPD thermostat and the AdResS force-coupling scheme (without the TD force extension) conserve strictly the local and total linear momentum (buffer + MD region), whereas the OBMD transfers the desired momentum flux to the explicit region through the boundary domain. Extending the OBMD framework with the TD force, which is needed in our case, means that we are applying an external force to the system, which changes the linear momentum (18). Thus, the linear momentum is not conserved on the local atomistic level, but it is conserved on the fluctuating hydrodynamics level of description, as was shown in (82). Note that our system is radially symmetric; therefore, the applied TD force is also symmetric over the center of the explicit region. Hence, for the homogeneous systems (e.g., salt solution), the total momentum would be, because of the symmetry (82), preserved on average even if the last term in Eq. 3 were omitted, i.e., $\tilde{\mathbf{F}}^{ext} = \mathbf{J} \cdot \mathbf{n}_B A + (\mathbf{P}_{out} - \mathbf{P}_{in})/\Delta t$. However, when the DNA molecule is added to the system, it disturbs the distributions of ions. As already demonstrated several times (11,67), counterions have a preferen-

tial binding to the DNA; thus, the distributions of ions are not radially symmetric around the DNA molecule. To prove this point, we show in Fig. 6 the density heat map of sodium and chloride ions in the plane normal to the DNA's long axis. To subtract the thermal rotation of the DNA molecule, we concurrently rotate all snapshots around the DNA long axis such that the DNA molecules can be superimposed. We can clearly see that there are specific angular regions around the DNA molecule with higher/lower ion concentrations, and the isotropic bulk densities are reached only at ~ 2.5 nm away from the DNA's CoM, i.e., beyond our explicit region. Because of this reason, the cumulative TD force (which for homogeneous systems on average cancels out) needs to be subtracted (Eq. 3) for the inhomogeneous systems.

In Fig. 7, we investigate the conservation of the total momentum, computed as a magnitude of the CoM velocity $V_{CoM} = \sum_i m_i |v_i| / \sum_i m_i$, where i runs over all water atoms and ions in the system. The results, obtained with Eq. 3, are compared with the case in which we omit the subtraction of the cumulative TD force ($\tilde{\mathbf{F}}^{ext}$). We can see that $\mathbf{F}^{ext}$ exactly preserves the global momentum for both systems, i.e., with and without the DNA molecule. On the other hand, using $\tilde{\mathbf{F}}^{ext}$ preserves on average the momentum for the salt solution system, whereas in the system containing DNA, the drifts in momentum are quite substantial. If the DNA molecule did not exhibit rotational diffusion around its long axis, this would show as a constant drift in a certain direction, which we would observe as a monotonically increasing V_{CoM}. However, because DNA naturally rotationally diffuses, the drift is fluctuating.

Impact of salt solution molarity on DNA molecule

The stability of the DNA molecule structure is examined by computing the root mean-square deviation (RMSD) and the root mean-square fluctuations (RMSFs) of the backbone atoms. Results are depicted in Fig. 8. The RMSDs and RMSFs are calculated with respect to the crystal structure that has the same sequence and was obtained from the Protein Data Bank (PDB: 196D). Under both salt solutions conditions, the DNA remains in the stable configuration during the total simulation run with approximately equal averages of RMSD and RMSF values. In contrast to the s.c. Odijk-Skolnick-Fixman effect, i.e., a long-range electrostatic stiffening of the DNA chain (83), our simulation results indicate that the DNA structure appears not to be significantly stiffened with increasing molarity. Moreover, the Odijk-Skolnick-Fixman effect cannot occur in our system because we impose a periodicity in the axial direction that fixes the helical pitch of DNA and therefore prevents any major bending fluctuations on the scale of the persistence length of the DNA molecule, approximately 50 nm, which is much larger than the single pitch. The use of a finite-length chain (intramolecular DNA interactions defined by bond, angle, and
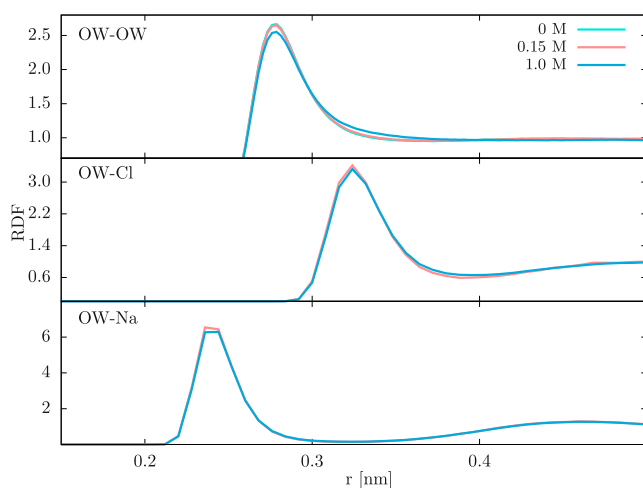

FIGURE 5 Radial distribution functions (RDFs) for the oxygen (OW), chloride (Cl), and sodium (Na) pairs. The notation is the same as in Fig. 3. To see this figure in color, go online.
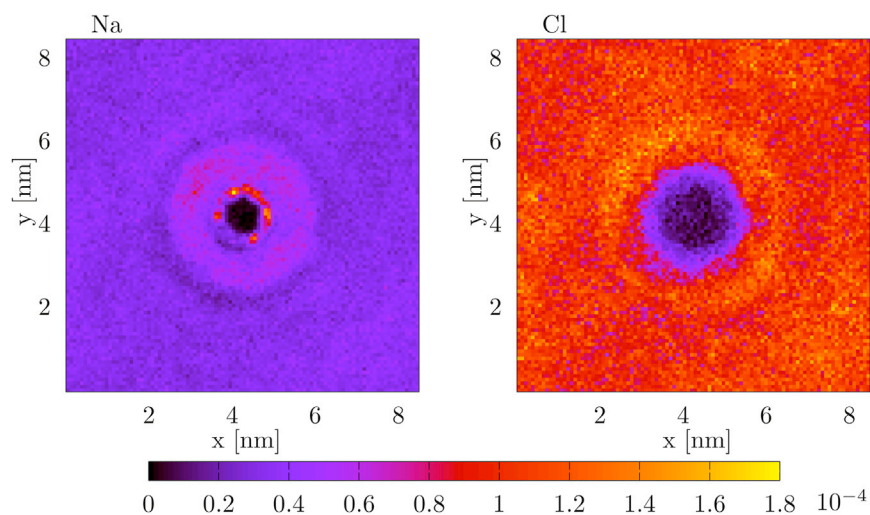
FIGURE 6 Density heat maps for sodium (Na) and chloride (Cl) ions in the plane normal to the DNA's long axis. Data are extracted from the closed all-atom simulation with 1 M NaCl salt solution (8). To see this figure in color, go online.

dihedral interaction potentials are used to connect each strand to its periodic image along the z axis) yields arguably a better approximation than that of the alternative case with no length constraint and with flexible terminal residues. Using four consecutive blocks of 5 ns from our production runs, the obtained RMSD block averages are 0.175, 0.172, and 0.181 for the 0.15 and 1.0 M OBMD simulations and the reference 1.0 M closed all-atom simulation (8), respectively. The corresponding SDs are 0.002, 0.004, and 0.005. These results demonstrate the simulation convergence with respect to time.

To further investigate the correlated motion of DNA atoms during simulation, we compute the dynamic cross-correlation map. The results for the DNA backbone atoms are plotted in Fig. 9. The cross-correlation coefficient of the covariance matrix is calculated as $A_{ij} = \langle \Delta x_i \Delta x_j \rangle / \sqrt{\langle \Delta x_i^2 \rangle \langle \Delta x_j^2 \rangle}$, where Δx_i and Δx_j correspond to the displacement of the ith and jth atoms from their mean position. The overall translational and rotational motion of the DNA needs to be removed before calculation. An increased level of correlated and anticorrelated motion is observed for the 1.0 M salt solution in comparison with the 0.15 M salt solution, which is again consistent with the fact that once electrostatics is eliminated, the local structure of a basepair depends on the type and structure of the flanking basepairs (84).
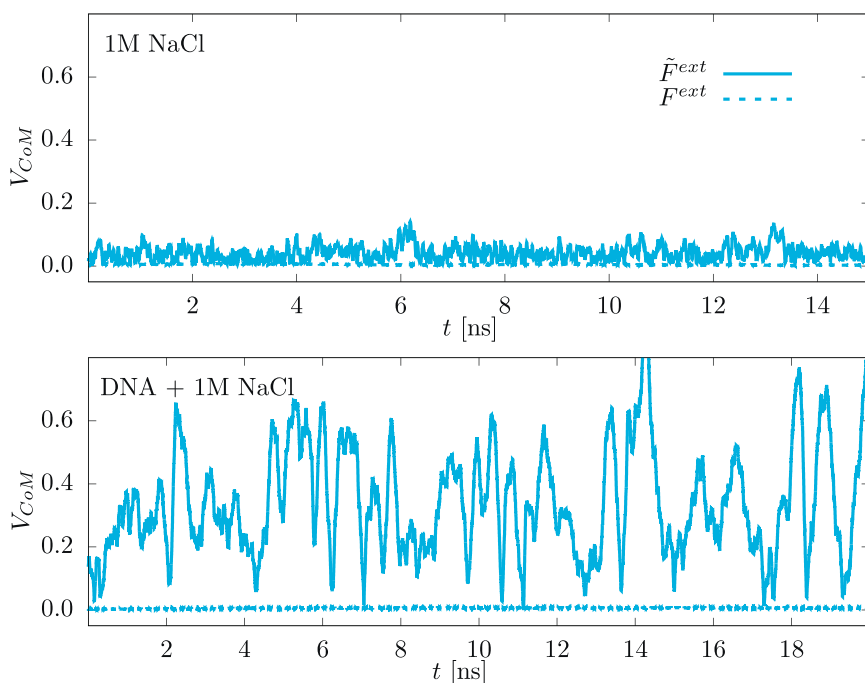

FIGURE 7 Magnitude of the total CoM velocity in units of nm/ps as a function of time for 1 M concentration without (*top*) and with the DNA molecule (*bottom*). We compare the results obtained with $\mathbf{F}^{ext}$ and $\tilde{\mathbf{F}}^{ext}$ defined in the text. To see this figure in color, go online.
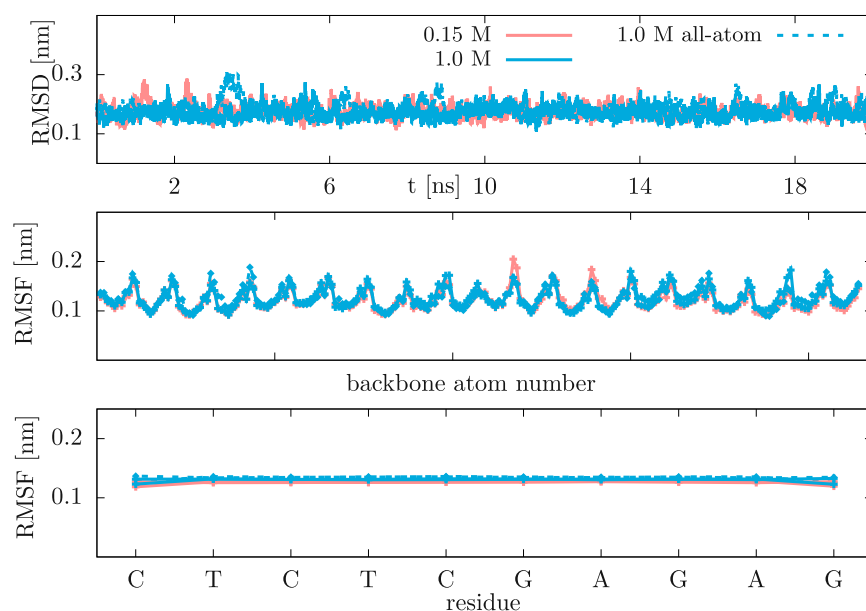
FIGURE 8 Root mean-square deviation (RMSD) and root mean-square fluctuations (RMSFs) of the backbone heavy atoms with respect to the crystal structure. The RMSFs are shown as a function of individual backbone heavy atoms and as a function of DNA nucleotides in which A, T, C, and G aberrations stand for the adenine, thymine, cytosine, and guanine nucleotides, respectively. The OBMD results are shown for the 0.15 and 1.0 M NaCl salt solutions and compared with the closed all-atom simulation with 1.0 M NaCl salt solution from (8). To see this figure in color, go online.

Finally, we show in Fig. 10 the charge compensation $Q(r)$ as a function of distance from the DNA's CoM. For both solvations, Q is equal to zero at $r = 0$ and increases with distance, reaching the unity at the bulk. For the 1 M salt solution, the charge is totally compensated at much smaller distances from the DNA. Notice also that for the 1 M solution, there is a peak at 1.8 nm from the CoM of DNA that is not encountered at the 0.15 M concentration.

CONCLUSIONS

We have presented the methodology for simulating biomolecules in a multiscale bathing solution, in which the explicit all-atom OBMD solvent model is coupled with the implicit solution model (implicit water with explicit ions). The OBMD technique enables one to incorporate into the model the transfer of mass, momentum, and energy across the boundaries of the studied molecular system. Such explicit-implicit coupling is especially compu-

tationally beneficial for simulations of systems that are sensitive to a salt concentration, such as biological polyelectrolytes. We applied the OBMD framework to simulate a DNA molecule at physiological (0.15 M) and ionic (1 M) conditions and showed that the ionic strength of the bathing solution impacts the properties of a DNA molecule. The significant computational speedup was achieved because of the absence of explicit water molecules in the implicit region. If the same systems were simulated with the vanilla all-atom MD, the systems would contain $\sim 67,800$ additional water atoms. Moreover, if one performed simulations at concentrations lower than that of the physiological, one would need to further enlarge the system, and the number of water molecules would be even greater. On the other hand, in our case, enlarging the implicit water part of the system has almost no computational overhead.

In this study, the subdomain of water is grand canonical, whereas the ions and DNA are kept at a fixed number. The
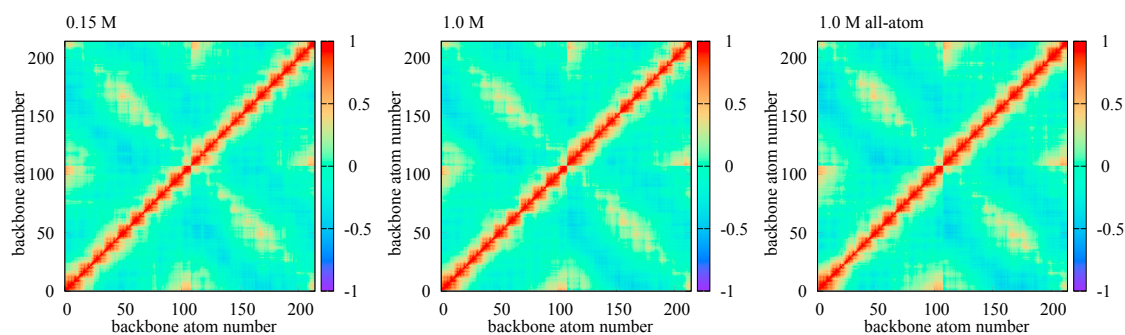

FIGURE 9 Dynamic cross-correlation maps for the DNA backbone heavy atoms. The notation is the same as in Fig. 8. To see this figure in color, go online.
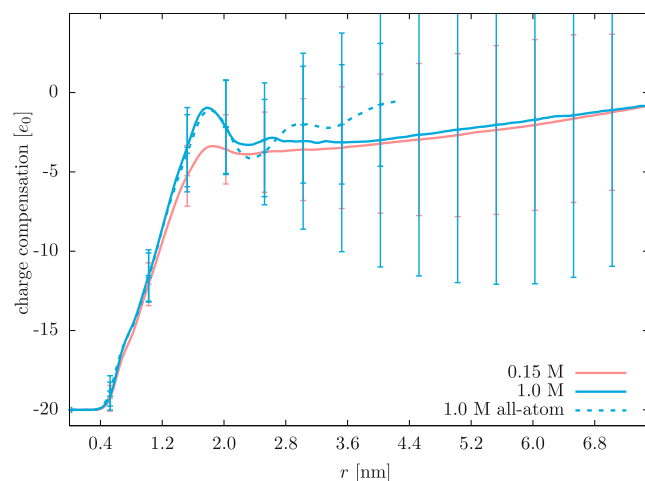
FIGURE 10 Charge compensation as a function of distance from the DNA's CoM. The notation is the same as in Fig. 8. To see this figure in color, go online.

overall ensemble is thus semi-grand-canonical. Employing the same methodology, we could also allow for the ion number to fluctuate. However, because of the unforeseen artifacts that could arise by the insertion of ions close to the DNA, we opted instead for a larger implicit water region, leading in fact to the same effect. We focused here on the equilibrium simulations, but arbitrary external boundary conditions could be imposed that would just as well permit the simulation of nonequilibrium dynamics (59). The framework presented could be used furthermore as an interface to connect MD with continuum hydrodynamics (85–94).

AUTHOR CONTRIBUTIONS

J.Z. and J.S. performed the simulations, and all the authors wrote the manuscript.

ACKNOWLEDGMENTS

REFERENCES

1. Leckband, D., and J. Israelachvili. 2001. Intermolecular forces in biology. *Q. Rev. Biophys.* 34:105–267.

2. Gelbart, W. M., R. F. Bruinsma, …, V. A. Parsegian. 2000. Like-charge attractions, however, have been observed in a variety of systems. *Phys. Today.* 53:38–44.

3. Simonson, T. 2003. Electrostatics and dynamics of proteins. *Rep. Prog. Phys.* 66:737–787.

4. Wong, G. C., and L. Pollack. 2010. Electrostatics of strongly charged biological polymers: ion-mediated interactions and self-or-ganization in nucleic acids and proteins. *Annu. Rev. Phys. Chem.* 61:171–189.

5. Allahyarov, E., G. Gompper, and H. Löwen. 2004. Attraction between DNA molecules mediated by multivalent ions. *Phys. Rev. E Stat. Nonlin. Soft Matter Phys.* 69:041904.

6. Biswas, M., J. Langowski, and T. C. Bishop. 2013. Atomistic simulations of nucleosomes. *WIREs Comput. Mol. Sci.* 3:378–392.

7. Voltz, K., J. Trylska, …, J. Langowski. 2012. Unwrapping of nucleosomal DNA ends: a multiscale molecular dynamics study. *Biophys. J.* 102:849–858.

8. Zavadlav, J., R. Podgornik, and M. Praprotnik. 2015. Adaptive resolution simulation of a DNA molecule in salt solution. *J. Chem. Theory Comput.* 11:5035–5044.

9. Stanley, C., and D. C. Rau. 2011. Evidence for water structuring forces between surfaces. *Curr. Opin. Colloid Interface Sci.* 16:551–556.

10. Bagchi, B. 2012. From anomalies in neat liquid to structure, dynamics and function in the biological world. *Chem. Phys. Lett.* 529:1–9.

11. Gavryushov, S. 2008. Electrostatics of B-DNA in NaCl and CaCl2 solutions: ion size, interionic correlation, and solvent dielectric saturation effects. *J. Phys. Chem. B.* 112:8955–8965.

12. Frauenfeldera, H., G. Chena, …, R. D. Young. 2003. A unified model of protein dynamics. *Proc. Natl. Acad. Sci. USA.* 106:5129–5134.

13. Lipfert, J., S. Doniach, …, D. Herschlag. 2014. Understanding nucleic acid-ion interactions. *Annu. Rev. Biochem.* 83:813–841.

14. Abrams, C. F. 2005. Concurrent dual-resolution Monte Carlo simulation of liquid methane. *J. Chem. Phys.* 123:234101.

15. Praprotnik, M., L. Delle Site, and K. Kremer. 2005. Adaptive resolution molecular-dynamics simulation: changing the degrees of freedom on the fly. *J. Chem. Phys.* 123:224106.

16. Praprotnik, M., L. D. Site, and K. Kremer. 2008. Multiscale simulation of soft matter: from scale bridging to adaptive resolution. *Annu. Rev. Phys. Chem.* 59:545–571.

17. Fritsch, S., S. Poblete, …, K. Kremer. 2012. Adaptive resolution molecular dynamics simulation through coupling to an internal particle reservoir. *Phys. Rev. Lett.* 108:170602.

18. Delle Site, L., and M. Praprotnik. 2017. Molecular systems with open boundaries: theory and simulation. *Phys. Rep.* 693:1–56.

19. Zavadlav, J., S. Bevc, and M. Praprotnik. 2017. Adaptive resolution simulations of biomolecular systems. *Eur. Biophys. J.* 46:821–835.

20. Wang, H., C. Hartmann, …, L. Delle Site. 2013. Grand-canonical-like molecular-dynamics simulations by using an adaptive-resolution technique. *Phys. Rev. X.* 3:011018.

21. Agarwal, A., and L. Delle Site. 2015. Path integral molecular dynamics within the grand canonical-like adaptive resolution technique: simulation of liquid water. *J. Chem. Phys.* 143:094102.

22. Delle Site, L. 2016. Formulation of Liouville's theorem for grand ensemble molecular simulations. *Phys. Rev. E.* 93:022130.

23. Delle Site, L. 2018. Grand canonical adaptive resolution simulation for molecules with electrons: a theoretical framework based on physical consistency. *Comput. Phys. Commun.* 222:94–101.

24. Potestio, R., S. Fritsch, …, D. Donadio. 2013. Hamiltonian adaptive resolution simulation for molecular liquids. *Phys. Rev. Lett.* 110:108301.

25. Potestio, R., P. Español, …, D. Donadio. 2013. Monte carlo adaptive resolution simulation of multicomponent molecular liquids. *Phys. Rev. Lett.* 111:060601.

26. Español, P., R. Delgado-Buscalioni, …, K. Kremer. 2015. Statistical mechanics of Hamiltonian adaptive resolution simulations. *J. Chem. Phys.* 142:064115.

27. Tarenzi, T., V. Calandrini, …, P. Carloni. 2017. Open boundary simulations of proteins and their hydration shells by Hamiltonian adaptive resolution scheme. *J. Chem. Theory Comput.* 13:5647–5657.

28. Everaers, R. 2016. Thermodynamic translational invariance in concurrent multiscale simulations of liquids. *Eur. Phys. J. Spec. Top.* 225:1483–1503.

29. Potoyan, D. A., A. Savelyev, and G. A. Papoian. 2013. Recent successes in coarse-grained modeling of DNA. *WIREs Comput. Mol. Sci.* 3:69–83.

30. Snodin, B. E. K., F. Randisi, …, J. P. K. Doye. 2015. Introducing improved structural properties and salt dependence into a coarse-grained model of DNA. *J. Chem. Phys.* 142:234901.

31. Maciejczyk, M., A. Spasic, …, H. A. Scheraga. 2014. DNA duplex formation with a coarse-grained model. *J. Chem. Theory Comput.* 10:5020–5035.

32. Knotts, T. A., IV, N. Rathore, …, J. J. de Pablo. 2007. A coarse grain model for DNA. *J. Chem. Phys.* 126:084901.

33. Voltz, K., J. Trylska, …, J. Smith. 2008. Coarse-grained force field for the nucleosome from self-consistent multiscaling. *J. Comput. Chem.* 29:1429–1439.

34. Bevc, S., C. Junghans, …, M. Praprotnik. 2013. Adaptive resolution simulation of salt solutions. *New J. Phys.* 15:105007.

35. Zavadlav, J., M. N. Melo, …, M. Praprotnik. 2014. Adaptive resolution simulation of MARTINI solvents. *J. Chem. Theory Comput.* 10:2591–2598.

36. Zavadlav, J., M. N. Melo, …, M. Praprotnik. 2015. Adaptive resolution simulation of polarizable supramolecular coarse-grained water models. *J. Chem. Phys.* 142:244118.

37. Zavadlav, J., S. J. Marrink, and M. Praprotnik. 2016. Adaptive resolution simulation of supramolecular water: the concurrent making, breaking, and remaking of water bundles. *J. Chem. Theory Comput.* 12:4138–4145.

38. Krekeler, C., and L. Delle Site. 2017. Towards open boundary molecular dynamics simulation of ionic liquids. *Phys. Chem. Chem. Phys.* 19:4701–4709.

39. Jabes, B. S., C. Krekeler, …, L. Delle Site. 2018. Probing spatial locality in ionic liquids with the grand canonical adaptive resolution molecular dynamics technique. *J. Chem. Phys.* 148:193804.

40. Lambeth, B. P., Jr., C. Junghans, …, L. Delle Site. 2010. Communication: on the locality of hydrogen bond networks at hydrophobic interfaces. *J. Chem. Phys.* 133:221101.

41. Zavadlav, J., M. N. Melo, …, M. Praprotnik. 2014. Adaptive resolution simulation of an atomistic protein in MARTINI water. *J. Chem. Phys.* 140:054114.

42. Fogarty, A. C., R. Potestio, and K. Kremer. 2015. Adaptive resolution simulation of a biomolecule and its hydration shell: structural and dynamical properties. *J. Chem. Phys.* 142:195101.

43. Kreis, K., R. Potestio, …, A. C. Fogarty. 2016. Adaptive resolution simulations with self-adjusting high-resolution regions. *J. Chem. Theory Comput.* 12:4067–4081.

44. Fogarty, A. C., R. Potestio, and K. Kremer. 2016. A multi-resolution model to capture both global fluctuations of an enzyme and molecular recognition in the ligand-binding site. *Proteins.* 84:1902–1913.

45. Netz, P. A., R. Potestio, and K. Kremer. 2016. Adaptive resolution simulation of oligonucleotides. *J. Chem. Phys.* 145:234101.

46. Zavadlav, J., R. Podgornik, and M. Praprotnik. 2017. Order and interactions in DNA arrays: multiscale molecular dynamics simulation. *Sci. Rep.* 7:4775–4786.

47. Guzman, H. V., C. Junghans, …, T. Stuehn. 2017. Scalable and fast heterogeneous molecular simulation with predictive parallelization schemes. *Phys. Rev. E.* 96:053311.

48. Kreis, K., A. Fogarty, …, R. Potestio. 2015. Advantages and challenges in coupling an ideal gas to atomistic models in adap- tive resolution simulations. *Eur. Phys. J. Spec. Top.* 224:2289–2304.

49. Martínez, L., and S. Shimizu. 2017. Molecular interpretation of preferential interactions in protein solvation: a solvent-shell perspective by means of minimum-distance distribution functions. *J. Chem. Theory Comput.* 13:6358–6372.

50. Lake, P. T., and M. McCullagh. 2017. Implicit Solvation Using the Superposition Approximation (IS-SPA): an implicit treatment of the nonpolar component to solvation for simulating molecular aggregation. *J. Chem. Theory Comput.* 13:5911–5924.

51. Shao, Q., and W. Zhu. 2017. How well can implicit solvent simulations explore folding pathways? A quantitative analysis of α-helix bundle proteins. *J. Chem. Theory Comput.* 13:6177–6190.

52. Luchko, T., S. Gusarov, …, A. Kovalenko. 2010. Three-dimensional molecular theory of solvation coupled with molecular dynamics in Amber. *J. Chem. Theory Comput.* 6:607–624.

53. Dixit, P. D., A. Bansal, …, D. Asthagiri. 2017. Mini-grand canonical ensemble: chemical potential in the solvation shell. *J. Chem. Phys.* 147:164901.

54. Jarzynski, C. 2017. Stochastic and macroscopic thermodynamics of strongly coupled systems. *Phys. Rev. X.* 7:011008.

55. Strasberg, P., G. Schaller, and T. Brandes. 2017. Quantum and information thermodynamics: a unifying framework based on repeated interactions. *Phys. Rev. X.* 7:011003.

56. Ouldridge, T. E., C. C. Govern, and P. Rein ten Wolde. 2017. Thermodynamics of computational copying in biochemical systems. *Phys. Rev. X.* 7:021004.

57. Ciliberto, S. 2017. Experiments in stochastic thermodynamics: short history and perspectives. *Phys. Rev. X.* 7:021051.

58. Delgado-Buscalioni, R., J. Sablić, and M. Praprotnik. 2015. Open boundary molecular dynamics. *Eur. Phys. J. Spec. Top.* 224:2331–2349.

59. Sablić, J., M. Praprotnik, and R. Delgado-Buscalioni. 2016. Open boundary molecular dynamics of sheared star-polymer melts. *Soft Matter.* 12:2416–2439.

60. Sablić, J., M. Praprotnik, and R. Delgado-Buscalioni. 2017. Deciphering the dynamics of star molecules in shear flow. *Soft Matter.* 13:4971–4987.

61. Sablić, J., R. Delgado-Buscalioni, and M. Praprotnik. 2017. Application of the Eckart frame to soft matter: rotation of star polymers under shear flow. *Soft Matter.* 13:6988–7000.

62. Flekkøy, E. G., R. Delgado-Buscalioni, and P. V. Coveney. 2005. Flux boundary conditions in particle simulations. *Phys. Rev. E Stat. Nonlin. Soft Matter Phys.* 72:026703.

63. Delgado-Buscalioni, R. 2012. Numerical Analysis of Multiscale Computations. Lecture Notes in Computational Science and Engineering, Volume 82. B. Engquist, O. Runborg, and Y. H. Tsai, eds. Springer, p. 145166.

64. Chu, V. B., Y. Bai, …, S. Doniach. 2008. A repulsive field: advances in the electrostatics of the ion atmosphere. *Curr. Opin. Chem. Biol.* 12:619–625.

65. Subirana, J. A., and M. Soler-López. 2003. Cations as hydrogen bond donors: a view of electrostatic interactions in DNA. *Annu. Rev. Biophys. Biomol. Struct.* 32:2745.

66. Draper, D. E., D. Grilley, and A. M. Soto. 2005. Ions and RNA folding. *Annu. Rev. Biophys. Biomol. Struct.* 34:221–243.

67. Bai, Y., M. Greenfeld, …, D. Herschlag. 2007. Quantitative and comprehensive decomposition of the ion atmosphere around nucleic acids. *J. Am. Chem. Soc.* 129:14981–14988.

68. Podgornik, R., J. Zavadlav, and M. Praprotnik. 2018. Molecular dynamics simulation of high density DNA arrays. *Computation.* 6:3.

69. Podgornik, R., M. A. Aksoyoglu, …, V. A. Parsegian. 2016. DNA equation of state: in vitro vs in viro. *J. Phys. Chem. B.* 120:6051–6060.

70. Duan, Y., C. Wu, …, P. Kollman. 2003. A point-charge force field for molecular mechanics simulations of proteins based on condensed-phase quantum mechanical calculations. *J. Comput. Chem.* 24:1999–2012.

71. Jorgensen, W. L., J. Chandrasekhar, …, M. L. Klein. 1983. Comparison of simple potential functions for simulating liquid water. *J. Chem. Phys.* 79:926–935.

72. Poblete, S., M. Praprotnik, …, L. Delle Site. 2010. Coupling different levels of resolution in molecular simulations. *J. Chem. Phys.* 132:114101.

73. Praprotnik, M., S. Poblete, and K. Kremer. 2011. Statistical physics problems in adaptive resolution computer simulations of complex fluids. *J. Stat. Phys.* 145:946–966.

74. Zavadlav, J., R. Podgornik, …, M. Praprotnik. 2016. Adaptive resolution simulation of an atomistic DNA molecule in MARTINI salt solution. *Eur. Phys. J. Spec. Top.* 225:1595–1607.

75. De Fabritiis, G., R. Delgado-Buscalioni, and P. V. Coveney. 2004. Energy controlled insertion of polar molecules in dense fluids. *J. Chem. Phys.* 121:12139–12142.

76. Halverson, J. D., T. Brandes, …, D. Reith. 2013. ESPResSo++: a modern multiscale simulation package for soft matter systems. *Comput. Phys. Commun.* 184:1129–1149.

77. Andersen, H. C. 1983. RATTLE: a "Velocity" version of the SHAKE algorithm for molecular dynamics calculations. *J. Comput. Phys.* 52:24–34.

78. Miyamoto, S., and P. A. Kollman. 1992. SETTLE: an analytical version of the SHAKE and RATTLE algorithm for rigid water models. *J. Comput. Chem.* 13:952–962.

79. Tironi, I. G., R. Sperb, …, W. F. van Gunsteren. 1995. A generalized reaction field method for molecular dynamics simulations. *J. Chem. Phys.* 102:5451–5459.

80. Vega, C., and J. L. F. Abascal. 2011. Simulating water with rigid non-polarizable models: a general perspective. *Phys. Chem. Chem. Phys.* 13:19663–19688.

81. Holzmann, J., R. Ludwig, …, D. Paschek. 2007. Pressure and salt effects in simulated water: two sides of the same coin? *Angew. Chem. Int. Ed.* 46:8907–8911.

82. Zavadlav, J., and M. Praprotnik. 2017. Adaptive resolution simulations coupling atomistic water to dissipative particle dynamics. *J. Chem. Phys.* 147:114110.

83. Cherstvy, A. G. 2011. Electrostatic interactions in biological DNA-related systems. *Phys. Chem. Chem. Phys.* 13:9942–9968.

84. Lavery, R., K. Zakrzewska, …, J. Sponer. 2010. A systematic molecular dynamics study of nearest-neighbor effects on base pair and base pair step conformations and fluctuations in B-DNA. *Nucleic Acids Res.* 38:299–313.

85. Delgado-Buscalioni, R., K. Kremer, and M. Praprotnik. 2008. Concurrent triple-scale simulation of molecular liquids. *J. Chem. Phys.* 128:114110.

86. Delgado-Buscalioni, R., K. Kremer, and M. Praprotnik. 2009. Coupling atomistic and continuum hydrodynamics through a mesoscopic model: application to liquid water. *J. Chem. Phys.* 131:244107.

87. Walther, J. H., M. Praprotnik, …, P. Koumoutsakos. 2012. Multiscale simulation of water flow past a C540 fullerene. *J. Comput. Phys.* 231:2677–2681.

88. Fabritiis, G. D., R. Delgado-Buscalioni, and P. V. Coveney. 2006. Modelling the mesoscale with molecular specificity. *Phys. Rev. Lett.* 97:134501.

89. De Fabritiis, G., M. Serrano, …, P. V. Coveney. 2007. Fluctuating hydrodynamic modeling of fluids at the nanoscale. *Phys. Rev. E Stat. Nonlin. Soft Matter Phys.* 75:026307.

90. Delgado-Buscalioni, R., and G. De Fabritiis. 2007. Embedding molecular dynamics within fluctuating hydrodynamics in multiscale simulations of liquids. *Phys. Rev. E Stat. Nonlin. Soft Matter Phys.* 76:036709.

91. Petsev, N. D., L. G. Leal, and M. S. Shell. 2015. Hybrid molecular-continuum simulations using smoothed dissipative particle dynamics. *J. Chem. Phys.* 142:044101.

92. Alekseeva, U., R. G. Winkler, and G. Sutmann. 2016. Hydrodynamics in adaptive resolution particle simulations: multiparticle collision dynamics. *J. Comput. Phys.* 314:1434.

93. Scukins, A., D. Nerukh, …, A. Markesteijn. 2015. Multiscale molecular dynamics/hydrodynamics implementation of two dimensional "Mercedes Benz" water model. *Eur. Phys. J. Spec. Top.* 224:2217–2238.

94. Qi, S., and F. Schmid. 2017. Hybrid particle-continuum simulations coupling Brownian dynamics and local dynamic density functional theory. *Soft Matter.* 13:7938–7947.